Advances in Radiation Oncology (2019) **4**, 233-236

advances
in radiation oncology

www.advancesradonc.org

Teaching Case

First Reported Case of Pediatric Radiation Treatment With Magnetic Resonance Image Guided Radiation Therapy

Lauren E. Henke MD, MSCI, Olga L. Green PhD, Joshua Schiff BS, Vivian L. Rodriguez PhD, Sasa Mutic PhD, Jeff Michalski MD, MBA, Stephanie M. Perkins MD*

Department of Radiation Oncology, Washington University School of Medicine, St. Louis, Missouri

Received 14 November 2018; accepted 23 January 2019

Introduction

Magnetic resonance (MR) image (MRI) guided radiation therapy (MRgRT) confers superior daily soft-tissue target visualization for many anatomic sites compared with traditional computed tomography (CT)—based radiation therapy and is increasingly used to manage inter- and intrafraction motion in a variety of cancer diagnoses.[1,2] There is growing evidence that MRgRT may be used to improve the dosimetric therapeutic index of radiation treatment through improved daily setup accuracy, the opportunity for daily online plan adaptation, and real-time cine MRI tumor motion tracking with beam gating.[3] In pediatric patients with cancer, unique emphasis is placed on maximization of the therapeutic index to minimize long-term risks of normal tissue exposure while maximizing durable disease control. Additionally, the young pediatric population is unable to actively participate in respiratory breath-hold treatment techniques for motion management, presenting an additional challenge and concern for treatment. Herein, we report the first use of MRgRT to treat a pediatric patient in the case of a 3-year-old girl with rhabdomyosarcoma. In addition, we describe key technical considerations of MRgRT use for maximization of safety, setup accuracy, and intrafraction motion management for the definitive treatment of a primary tumor of the diaphragm in a small child.

Case

A 3-year-old girl presented with sleep difficulty and 5 days of abdominal distention with urinary retention. A CT of the chest and abdomen identified a 17 × 10 cm mass centered at the diaphragm, with mass effect on the liver and direct extension into the anterior mediastinum, with a mediastinal component measuring 7 cm × 2.7 cm with compression of the right ventricle (Fig. 1). Subsequent ultrasound guided biopsy revealed a diagnosis of embryonal rhabdomyosarcoma on histopathologic analysis, with immunohistochemistry staining positive for vimentin and desmin. Fluorescence in situ hybridization revealed no evidence for a *FOXO1*-containing chromosomal rearrangement. Positron emission tomography—CT imaging and bilateral bone marrow biopsy indicated no evidence of additional distant metastatic disease. These

Sources of support: This work had no specific funding.

Conflicts of interest: Dr Henke reports grants and personal fees from ViewRay, Inc, outside the submitted work and grants from Varian Medical Systems outside the submitted work. Dr Green reports personal fees and other from ViewRay, Inc, outside the submitted work. Dr Mutic reports grants and other from ViewRay, Inc; grants and other from Varian Medical Systems; other from Philips Healthcare; other from Siemens; other from TreatSafely, LLC; and other from Radialogica, LLC, outside the submitted work.

* Corresponding author. Department of Radiation Oncology, Washington University School of Medicine, Campus Box 8224, 4921 Parkview Place, Floor LL, St. Louis, MO 63110.

E-mail address: sperkins@wustl.edu (S.M. Perkins).

https://doi.org/10.1016/j.adro.2019.01.008

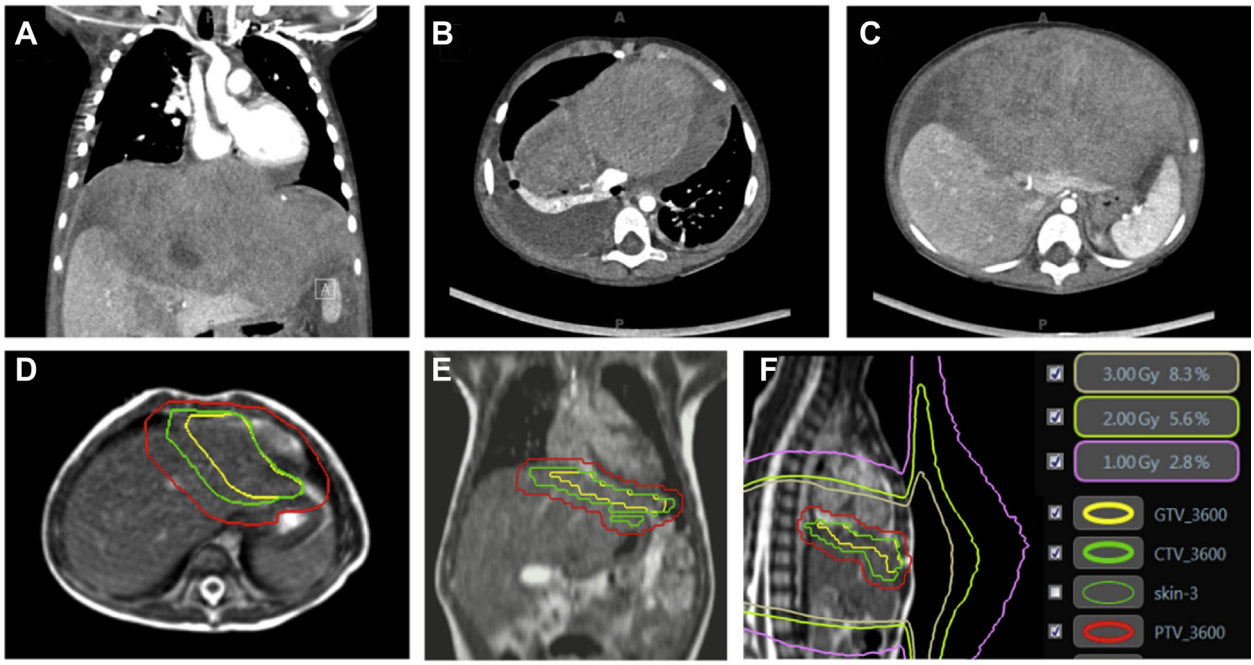

Fig. 1 (A-C) Diaphragmatic rhabdomyosarcoma tumor burden at time of diagnosis. (D and E) Gross target volume (yellow contour), clinical target volume (green contour), and planning target volume (red contour). (F) 1-, 2-, and 3-Gy isodose lines from the delivered treatment plan indicate curvature of low-dose isodose lines away from the body under the influence of the magnetic field, without dose return to the skin, to show lack of clinically significant electron return effect or magnetic field–induced dose distortions. *Abbreviations:* CTV = clinical target volume; GTV = gross tumor volume; PTV = planning target volume.

findings were consistent with intergroup rhabdomyosarcoma study group T2bN0M0 stage III disease of favorable histologic characteristics and unfavorable site.

The patient initiated a chemotherapy regimen including cycles of vincristine, ifosfamide, etoposide, dactinomycin, cyclophosphamide, irinotecan, and doxorubicin with filgrastim support. Interval CT imaging indicated a partial response to chemotherapy, and the patient subsequently underwent gross total surgical resection of her diaphragmatic and mediastinal disease. Histopathologic examination revealed a 5.8 × 5.3-cm primary diaphragmatic tumor with evidence of treatment response and negative margins, containing a small residual focus of viable embryonal rhabdomyosarcoma and no evidence of residual mediastinal disease. Postoperative CT indicated no evidence of residual or metastatic disease. The patient reinitiated chemotherapy and was referred to radiation oncology to consider adjuvant radiation therapy with concurrent chemotherapy.

Considering the pathology findings from surgery, a recommendation was made that the primary tumor site involving the diaphragm be treated with radiation therapy to a total dose of 36 Gy in 20 daily fractions of 1.8 Gy using intensity modulated radiation therapy. MR guidance was selected for maximal setup accuracy and intrafraction motion management without the additional imaging dose inherent to CT-guided treatment paradigms with kilovoltage-based on-board imaging. Given the young age of the patient, daily anesthesia was required for all treatment fractions.

Treatment Planning and Delivery

Detailed descriptions of the initial planning process, simulation, and MRgRT treatment device, including its imaging characteristics and dedicated treatment planning system (TPS), have been previously published.[4-7] For this pediatric patient, simulation comprised both CT and MRI, with use of CT as the primary data set. The gross tumor volume (GTV) was defined as the preoperative visible tumor volume with modifications accounting for return of organs to their normal anatomic position after surgery. The clinical target volume (CTV) comprised a 1 cm volumetric expansion on the GTV, with modification for extension into normal organs (eg, heart). The planning target volume (PTV) was created using a 0.5 cm volumetric expansion on the CTV. Treatment target volumes are shown in Figure 1.

Motion of the target volume was evaluated with use of 4-dimensional CT at the time of simulation. Imaging indicated movement of the target with breathing. Given the patient's age, there was no ability to employ a breath-hold technique for treatment; the decision was made to proceed with real-time cine MR beam gating, which has been previously described in the literature,[8] and no

Table 1 In vivo peripheral dose measurements with optically stimulated luminescence dosimeters for chin, pelvis, and breast areas

Measurement point	Measured dose per fraction (cGy)	Total dose for 20 fractions (cGy)	TPS predicted total dose (cGy)	Difference between TPS and measurement (%)
Chin 1	2.04	40.8	-	-
Chin 2	2.03	40.6	-	-
Chin 3	2.05	41	-	-
Pelvis 1	0.81	16.2	-	-
Pelvis 2	0.85	17	-	-
Pelvis 3	0.86	17.2	-	-
Breast (average of 2 highest measurements)	109.13	2182.6	2242.5	−2.70%

Abbreviation: TPS = treatment planning system.
Comparisons with the treatment planning system predictions are shown where available.

additional PTV motion margin was required. Prescribed dose to the PTV was 36 Gy in 20 fractions of 1.80 Gy each. Step-and-shoot intensity modulated radiation therapy planning was completed using the dedicated TPS of the MRgRT system.

Briefly, the hybrid MRgRT system used for this patient consists of a split-solenoid 0.35-T superconducting magnet, with 3 co-rotating cobalt-60 sources equally distributed, mounted on a gantry sandwiched by the magnet. Multileaf collimators positioned under each source provide beam shaping and full shielding. The system can deliver from all 3 sources simultaneously while imaging in the sagittal plane at a rate of 4 frames per second. The presence of the magnetic field is taken into account during treatment planning by the Monte Carlo–based TPS integrated in the MRgRT device. For this pediatric patient, the presence of the magnetic field during treatment presented 2 concerns. The first was the effect of the magnetic field on the dose distribution both inside and outside the patient. The second was the need for anesthesia monitoring equipment, for which the vault housing the MRgRT system was not initially designed.

Regarding the first of these concerns, previous publications have reported that the 0.35-T magnetic field has little effect on dose deposition in soft tissue, where the mean free path of secondary electrons is too short to be curved by the Lorentz force.[9] However, as the beam exits the patient, secondary electrons created at the exit surface into air are indeed curved toward a path along the body, potentially impinging on other parts of the body such as, in this case, the chin.[10] In vivo dosimetry measurements were performed during the first 2 fractions of therapy to evaluate the peripheral doses in 3 areas: the chin, the pelvis, and breast (site of particular exposure concern near the treatment area). Optically stimulated luminescence dosimeters (Microstar-II, Landauer, Inc, Glenwood, IL) were placed on the patient's body and read out immediately after delivery. Based on these measurements, the chin and pelvis were estimated to receive about 1% and 0.5% of the total prescription dose, respectively, comparable to peripheral surface doses from standard linear accelerators (Fig. 1). Comparison with TPS prediction was made for the optically stimulated luminescence dosimeters placed near the breast; however, the chin and pelvis were outside the planning image data set and therefore outside the calculation grid. The 2 maximum points measured for the breast were within 3% of the TPS prediction. Detailed results are presented in Table 1.

Special considerations were also required in this case for MR-compatible treatment monitoring. The hospital's anesthesia team was present for every fraction, and although their monitoring equipment was MR compatible, it was not possible to see it inside the room with the existing patient camera system. A standalone camera with a tripod was acquired and connected to a laptop computer placed in the radiofrequency insulated equipment closet inside the treatment vault. An ethernet cable from this laptop was fed via a filter panel in the equipment closet to another laptop outside the treatment area, thus eliminating the concern of reduced MR image quality from monitoring equipment–produced radiofrequency noise. Preliminary testing was performed with this equipment set up and a homogenous, liquid spherical phantom to evaluate the signal-to-noise ratio compared with baseline; no change in signal-to-noise ratio was detected.

All treatment fractions were delivered with a custom immobilization device and real-time MR guidance, including cine MR gating on the target volume, based on the exhale phase during free breathing, using the described monitoring for daily sedation. At time of clinical setup for each treatment fraction, the patient underwent high-resolution volumetric MRI at exhale-breath-hold in the treatment position and was then aligned to the GTV to maximize plan/tumor overlap. Gating window targets and settings were selected by the treating physician and evaluated on each treatment day.

Details of MR guidance with cine MR gating, as implemented at our institution for standard clinical practice, have been previously published.[8]

The decision to proceed with MRgRT resulted in improved sparing of normal tissues. As described earlier, a 0.5-cm CTV to PTV expansion was used in this case to better account for intrafraction motion via real-time cine MRI beam gating on the target. Had the patient been treated without MR guidance for motion management (using standard cone beam CT–based image guidance instead), the comparison-planned PTV expansion would have been 1.0 cm because of the need to account for both respiratory motion of the diaphragmatic target and setup uncertainty. This would have resulted in a 59% larger PTV volume (357.8 cm^3 vs the 224.8 cm^3 PTV volume treated here). Thus, 133 cm^3 more normal tissue, including the adjacent diaphragm, lungs, liver, and heart, would have been treated in the absence of MRgRT technology, given that any additional PTV expansion would comprise a hollow sphere of additional normal tissue around the target (357.8 cm^3 − 224.8 cm^3 = 133 cm^3).

Regarding treatment outcome, the patient tolerated all treatment fractions without identified acute toxicity. Specifically, she had no nausea, vomiting, or diarrhea during or immediately after radiation treatment; her parents noted only mild fatigue. At 28 months after radiation, the patient remained without evidence of local or distant disease recurrence and without identified late toxicity attributable to radiation treatment.

Conclusions

This is the first described clinical use of MRgRT for a pediatric patient. In this reported case, MRgRT was used to maximize soft-tissue visualization and daily setup accuracy while optimizing the management of motion in a highly mobile (diaphragmatic) disease site to minimize treatment volumes. Delivery of MRgRT to a pediatric patient requires several unique technical considerations, including the use of MR-compatible anesthetic monitoring, but has been successfully and safely accomplished in a routine clinical setting. As MRgRT enters widespread clinical use, indications in the pediatric population for applications such as online adaptive radiation therapy and motion management to better spare normal tissues while maintaining target coverage are likely to expand.

References

1. Noel CE, Parikh PJ, Spencer CR, et al. Comparison of onboard low-field magnetic resonance imaging versus onboard computed tomography for anatomy visualization in radiation therapy. *Acta Oncol*. 2015;54:1474-1482.
2. Fischer-Valuck BW, Henke LE, Green O, et al. Two-and-a-half-year clinical experience with the world's first magnetic resonance image guided radiation therapy system. *Adv Radiat Oncol*. 2017;2:485-493.
3. Henke L, Kashani R, Robinson CG, et al. Phase I trial of stereotactic MR-guided online adaptive radiation therapy (SMART) for the treatment of oligometastatic or unresectable primary malignancies of the abdomen. *Radiother Oncol*. 2018;126:519-526.
4. Hu Y, Rankine L, Green OL, et al. Characterization of the onboard imaging unit for the first clinical magnetic resonance image guided radiation therapy system. *Med Phys*. 2015;42:5828-5837.
5. Mutic S, Dempsey JF. The ViewRay system: Magnetic resonance-guided and controlled radiation therapy. *Semin Radiat Oncol*. 2014;24:196-199.
6. Yang D, Wooten HO, Green O, et al. A software tool to automatically assure and report daily treatment deliveries by a cobalt-60 radiation therapy device. *J Appl Clin Med Phys*. 2016;17:492-501.
7. Acharya S, Fischer-Valuck BW, Kashani R, et al. Online magnetic resonance image guided adaptive radiation therapy: First clinical applications. *Int J Radiat Oncol Biol Phys*. 2016;94:394-403.
8. Green OL, Rankine LJ, Cai B, et al. First clinical implementation of real-time, real anatomy tracking and radiation beam control. *Med Phys*. 2018 May 28. https://doi.org/10.1002/mp.13002. [Epub ahead of print].
9. Raaijmakers AJE, Raaymakers BW, Lagendijk JJW. Magnetic-field-induced dose effects in MR-guided radiotherapy systems: Dependence on the magnetic field strength. *Phys Med Biol*. 2008;53:909-923.
10. Hackett SL, van Asselen B, Wolthaus JWH, et al. Spiraling contaminant electrons increase doses to surfaces outside the photon beam of an MRI-linac with a perpendicular magnetic field. *Phys Med Biol*. 2018;63:095001-095011.